

# Report of the Short Term Scientific Mission: “An updated zenith sky retrieval algorithm” (ES1207-29577)

H. Diémoz<sup>1,2</sup>

<sup>1</sup>ARPA Valle d’Aosta, Saint-Christophe, Italy

<sup>2</sup>ISAC-CNR, Rome, Italy

November 9, 2015

## 1 Introduction

The Brewer spectrophotometer estimates the ozone content in the atmosphere in two different observation modes. In the direct sun (DS) geometry, which is the primary measurement mode, the Brewer directly points to the sun. This technique guarantees very high precision and accuracy and is equally sensitive to stratospheric and tropospheric fractions of the total ozone. Furthermore, the airmass factors (AMFs), describing the enhancement of the path in the atmosphere as a function of the solar zenith angle (SZA), are easy to calculate using geometrical considerations (up to AMF of about 5). Conversely, in the zenith sky (ZS) geometry the Brewer points to the zenith and records the diffuse (polarised) radiation reaching the ground from this direction. This mode is believed to be more sensitive to the stratospheric ozone compared to the tropospheric fraction, due to the enhanced path of the diffuse photons in the stratosphere (Solomon et al., 1987), and is considered to be less affected by the presence of clouds, thus allowing to compare satellite and ground-based instruments in cloudy scenarios and to generate long-term ozone time series unbiased by meteorological conditions.

The algorithm to retrieve ozone from zenith measurements was first developed by Dobson (1957) and is based on the so-called “zenith sky charts”, i.e. empirical functions describing the relation between the zenith radiance and the ozone content. For the Brewer, the algorithm is implemented using a set of nine empirical coefficients linking the ratios of the radiances measured at four different wavelengths to a quadratic function of the ozone vertical column density (VCD) and the AMF (Kerr et al., 1981) and determined through comparison between DS and ZS observations. To this purpose, a large dataset of nearly simultaneous measurements (usually, more than 500 pairs), possibly spanning the full operational range of AMFs and VCDs, must be available. In principle, every single Brewer requires a different set of polynomial coefficients for optimised zenith sky total ozone retrievals, owing to slightly different instrumental characteristics (Muthama et al., 1995).

Fioletov et al. (2011) updated this method on the basis of radiative transfer models (RTMs). The authors calculated an initial set of nine coefficients based on simulations (and thus, dependent on the characteristics of the atmosphere), that were then adapted to a specific instrument by tuning two additional scaling factors. The method still relies on the empirical, quadratic relationship of the AMF and the ozone VCD and involves comparison between DS and ZS measurements, but a much smaller set of nearly simultaneous data is required compared to the classic algorithm.

Although those recent advances had allowed to remarkably improve the comparison between DS and ZS estimates and decrease their relative difference down to few percentage points, some issues still deserve attention. First, the current approaches lack of a formal description of the underlying physics, such as the Bouguer-Lamber-Beer law in the DS case (e.g., Bouguer, 1729). Therefore, ZS retrievals can only be performed when reference measurements, i.e. DS observations, are available and don’t provide any further information they may help to discover, or solve, DS inconsistencies (e.g., at very large SZAs). Moreover, ZS auto-calibrations, such as Langley extrapolations (Langley, 1880) in a pristine site, are not possible at present without defining a physical quantity equivalent to the DS AMF. Second, there is little understanding about the instrumental factors affecting the ZS retrieval, which are currently merged into the empirical relations between DS and ZS. For example, Fioletov et al. (2011) propose a linear correction to improve the ZS-DS comparison, but they do not provide any clear explanation about the underlying physics (e.g., they do not justify why two - and only two - correction factors are needed). To this aim, a new formulation decoupling the atmospheric and the instrumental effects is needed and further investigations must be carried out. Finally, the previous studies examine the behaviour of the ZS retrievals in the airmass range spanned by DS records, e.g. up to AMFs of about 6 (corresponding to SZAs of about 82 degrees). However, ZS measurements are often scheduled when the sun is very low on the horizon and DS observations

are difficult or not possible (e.g., during winter at high latitudes or everywhere during twilight), therefore a detailed characterisation of the method in this range is necessary.

The following topics were studied in the present work:

1. a formal, mathematical description of the physics underlying the observations along the zenith direction is provided;
2. zenith sky measurements were performed during a 15-days calibration campaign at Mauna Loa Observatory (MLO), Hawaii since September 24, 2015 to October 8;
3. radiative transfer simulations were carried out using a full-spherical model simulating the response by a Brewer. To this purpose, the actual operating wavelengths and bandwidths of the Brewers participating to the campaign were provided as inputs to the model and the linear combination (R6) of the simulated irradiances was calculated as a function of the ozone VCD and the SZA. Polarisation was included in the simulations, which distinguishes this work from the previous ones;
4. it is discussed whether (and under what conditions) it is possible to condense the complex physics of ZS radiative transfer to a simple function, i.e. an “effective” ZS AMF (as done, for instance, by Diémoz et al. (2014) for nitrogen dioxide). Indeed, due to the strong absorption by ozone at lower wavelengths, saturation and Umkehr effects are observed, which considerably complicate the ozone retrieval;
5. preliminary results of a zenith-sky Langley calibration, making use of the new formulation, are presented. This point allowed to calibrate the ZS observations independently from simultaneous DS measurements;
6. the algorithm performances are analysed at various wavelength ranges corresponding to several grating positions. Notably, the microstep normally employed for Umkehr observations at larger wavelengths was studied. At those wavelengths (about 327–336 nm), the ozone absorbs weakly, which allows a simpler formulation of the problem and an easy solution, especially at large slant column amounts;
7. finally, a new routine (`zu.rtn`) was developed and shared with the Brewer users community. The new routine operates in the larger wavelength range and turn the tracker perpendicularly to the sun to improve the accuracy of the measurements. Furthermore, since a higher number of photons are available at larger wavelengths, the algorithm can be modified to use all the six slits of a Brewer and the straylight is believed to decrease compared to

the lower wavelength range. These improvements could be especially valuable for measurements at high latitudes.

## 2 Problem formulation

In a purely scattering atmosphere, the spectral irradiance,  $I(\lambda, 0)$ , recorded by a Brewer pointing to the zenith is proportional to the incoming solar flux (corrected for the Earth-Sun distance),  $E(\lambda)$ , i.e.

$$I(\lambda, 0) = f(\lambda) E(\lambda) \quad (1)$$

The dependence on SZA was dropped for sake of simplicity.  $f(\lambda)$  stands for the fraction (probability) of  $E(\lambda)$  that is received by the detector for a scattering only, but not absorbing, atmosphere. The mathematical formulation by Marquard et al. (2000) can be adopted to describe an atmosphere that also includes an absorbing species, e.g. ozone:

$$I(\lambda, X) = I(\lambda, 0) \int d\Gamma p(\lambda, \Gamma) e^{-\int_{\Gamma} ds \sigma(\lambda, s) n(s)} \quad (2)$$

where  $X$  is the ozone VCD.  $p(\lambda, \Gamma)$  is the probability that a photon will follow the path  $\Gamma$  in the atmosphere before reaching the detector. This probability depends on both the wavelength of the radiation and the absorption and scattering properties of the atmosphere. The exponential term is the well-known Bouguer-Lambert-Beer (BLB) equation along the path  $\Gamma$ .  $s$  is the differential length in the path,  $\sigma(\lambda, s)$  the absorption cross section of ozone and  $n(s)$  the ozone number concentration. It is easy to prove that when the concentration of the absorber tends to zero, then Eq. 1 is obtained since the integral of the probability  $p$  must give unity. It must be noticed that Eq. 2 is different from the BLB law for the DS geometry:

$$I_{DS}(\lambda, X) = I_{DS}(\lambda, 0) e^{-\int dz \mu \sigma(\lambda, z) n(z)} \quad (3)$$

where the AMF,  $\mu$ , was introduced to use the vertical coordinate  $z$  instead of the slant path  $s$ .

We could wonder whether Eq. 3 can be fitted to Eq. 2, as frequently done when dealing with weak absorbers (e.g. Diémoz et al., 2014). If this were the case, the full physics could be included in a function  $\mu_{ZS}$  representing an “effective” AMF and depending only on the sun geometry and the scattering properties of the atmosphere, but not on the absorption. As we will prove further down in the text, this is not generally possible in the case of a strong absorber. Indeed, as shown by Marquard et al. (2000),  $\mu_{ZS}$  will depend on  $X$ .

As in the standard DS ozone retrieval algorithm, we can calculate the logarithm of Eq. 2 and linearly combine the measurements recorded through the Brewer slits at four different wavelengths:

$$\begin{aligned}
& \sum \gamma_i \log I(\lambda_i, X) = \\
& \sum \gamma_i \log I(\lambda_i, 0) + \\
& \sum \gamma_i \log \int d\Gamma p(\lambda_i, \Gamma) e^{-\int_{\Gamma} ds \sigma(\lambda_i, s) n(s)}
\end{aligned} \tag{4}$$

The weightings  $\gamma_i$  can be chosen to minimise the influence by constant factors, aerosols and sulphur dioxide (that we did not explicitly consider, for sake of simplicity, in the previous equations). We can write Eq. 4 in a shorter form:

$$F(\theta, X) = S(\theta) - G(\theta, X) \tag{5}$$

where the dependence on the SZA,  $\theta$ , was restored. The sign of  $G$  was chosen to remind that this is an extinction term, while  $S$  is a source term. An additional effect of the linear combination is that the Rayleigh scattering term is almost completely removed (since it is indistinguishable, in such a short wavelength interval, from the aerosol term), i.e.  $S$  is several orders of magnitude lower than  $F$  and  $G$  (Sect. 5) and can be neglected. However, since the function  $S$  is easy to calculate, we will keep the term and apply the Rayleigh compensation to the measurements anyway. In contrast with the DS case, it is worth repeating that  $G(\theta, X)$  is not a linear function of  $X$ .

By deriving Eq. 5, we obtain

$$\frac{dF(\theta, X)}{dX} = -\frac{dG(\theta, X)}{dX} \tag{6}$$

A measurement error in the linear combination,  $\Delta F$ , will propagate to ozone in the following way:

$$\Delta X = \frac{\Delta F}{-\frac{dG}{dX}} \tag{7}$$

Therefore, the term  $\frac{dG}{dX}$  - which, in the DS case, was linked to the airmass - represents the sensitivity of the algorithm to ozone variations. The larger the  $\frac{dG}{dX}$  term (for the same set of weighting factors), the better the ozone retrieval.

### 3 Radiative transfer model

The radiative transfer model SCIATRAN (Rozanov et al., 2014) was used to simulate the irradiance recorded by a Brewer and calculate the functions  $F$ ,  $S$  and  $G$ . This model, which was extensively validated, supports full-spherical geometry and polarisation. The model provides the four components of the Stokes vector, then the irradiance in both polarisation planes (i.e., parallel and perpendicular to the principal plane of scattering, i.e. the plane that includes the sun, the zenith and the Brewer) may be obtained using the following formulae:

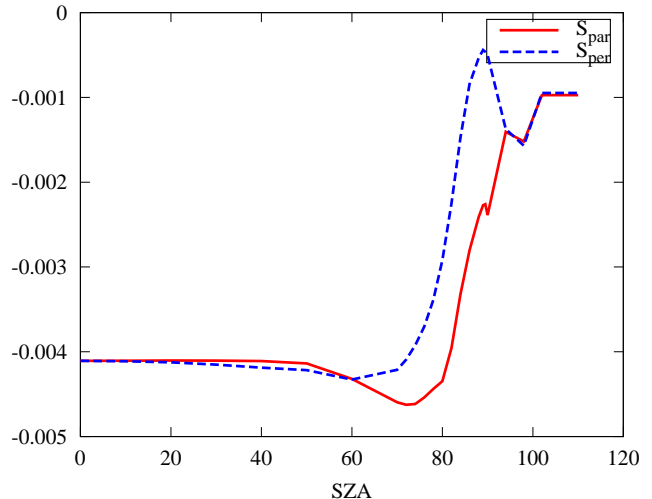


Figure 1:  $S$ , i.e. the linear combination of the intensity logarithms for a purely scattering atmosphere, in parallel and perpendicular polarisations as a function of the solar zenith angle for the MLO atmosphere.

$$I_{\parallel} = \frac{\mathcal{I} + \mathcal{Q}}{2} \tag{8}$$

$$I_{\perp} = \frac{\mathcal{I} - \mathcal{Q}}{2} \tag{9}$$

$\mathcal{I}$  and  $\mathcal{Q}$  being the first two components of the Stokes vector. The model was configured to simulate the Mauna Loa atmosphere at the moment of the measurements. The solar spectral irradiance was calculated at several wavelengths within the bandwidth of every Brewer slit (every 0.1 nm) and then convoluted with a trapezoidal function representing the slit function. The centre wavelengths and the bandwidths of every slit were determined from the dispersion tests during the campaign. To interpolate the data at the operating step, an accurate fitting function was used (Gröbner et al., 1998). Multiple scattering and refraction were included in the model. The surface albedo was initially set to 0.03 and the altitude to 3.4 km a.s.l. The Brewer Bass and Paur (1985) ozone cross sections were used. The vertical profiles at a latitude of 15°N from a climatological database obtained using a 2D chemo-dynamical model developed at MPI Mainz (Brühl and Crutzen, 1993) and included in SCIATRAN were chosen. Atmospheric pressure was scaled to 680 hPa. The ozone content (from 200 to 500 DU) and the SZA (from 0 to 110 degrees) were iteratively changed to determine  $S(\theta)$  and  $G(\theta, X)$ .

## 4 Measuring site and instruments

Due to its altitude and its atmospheric stability, the observatory of Mauna Loa, Hawaii (19.536°N, 155.576°W, 3400 m a.s.l.) represents the ideal site to test a retrieval algorithm and to calibrate a solar instrument (e.g., Slusser et al., 2000). Six Brewer spectrophotometers were operating during the campaign: two MkII models (#008 and #017), three MkIII (#119, #145 and #187) and one MkIV (#009). Such a unique variety allows comparison of the performances (e.g., stray-light) of different models. The campaign lasted from September 24, 2015 (day of year 267) to October 8 (day 281). The measurement schedules included some zenith sky observations during the day in both polarisations. Indeed, if the tracker is rotated towards the sun (**zs** routine), only the polarisation component parallel to the scattering plane is transmitted to the grating, while when the instrument is turned perpendicularly to the sun (**zp** routine), the component polarised perpendicularly to the scattering plane is detected. To quickly check this assumption, the corrected count rates from both polarisations were compared and, as expected, the perpendicular component is dominating at twilight. Usually, ZS measurements are performed with reference to the parallel component, since photons polarised in this direction at twilight mainly come from multiple scattering and therefore clouds exercise a smaller influence. In the final days, a new routine (**zu**) was developed and included in the schedules. The standard DS data reduction is performed on the raw counts: dark counts subtraction, conversion to count rates, dead time compensation and temperature compensation. Only the nominal attenuation of the neutral density filters (but not the real spectral attenuation) was considered in this preliminary analysis. The compensation for Rayleigh scattering was achieved by calculating and subtracting the function  $S(\theta)$  (Eq. 5) to the linear combination of the intensity logarithms.

## 5 Results

### 5.1 Zenith sky simulations

The function  $S$ , i.e. the linear combination of the intensity logarithms for a purely scattering atmosphere, is plotted in Fig. 1. The two polarisations show different behaviour, as a result of the different observation geometries relative to the scattering plane (e.g., photons in the parallel component mainly originate from multiple scattering). It can be observed that the value of  $S$  is several orders of magnitude lower than  $G$  (Figs. 2 and 3).

The matrix  $G$  in both polarisations is plotted in Figs. 2 and 3. The chart is drawn as a function of the direct AMF to allow an easy comparison to Fig. 1

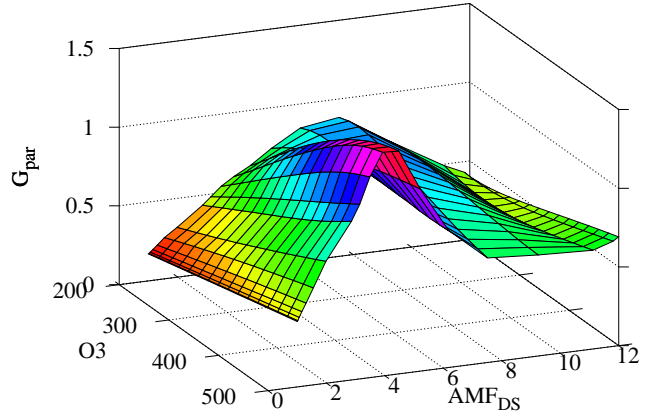


Figure 2: Matrix  $G$  in parallel polarisation, i.e. contribution of ozone (at different solar zenith angles) to the linear combination.

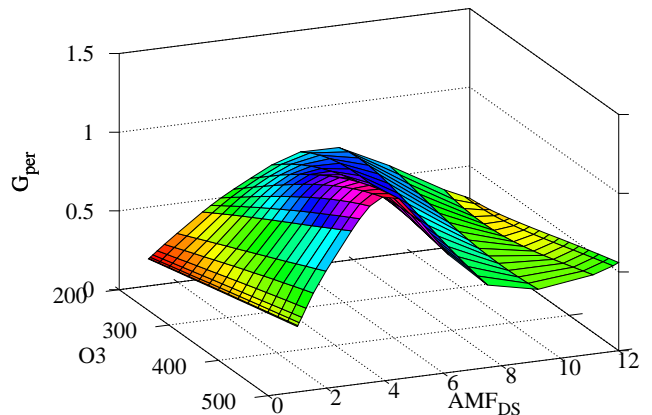


Figure 3: Matrix  $G$  in perpendicular polarisation, i.e. contribution of ozone (at different solar zenith angles) to the linear combination.

in the article by Fioletov et al. (2011) (who call the linear combination  $G$  instead of  $F$ ). However, since the Rayleigh contribution is mostly removed by the choice of the weightings, the two matrices almost coincide). To calculate DS AMFs, only  $\text{SZA} < 90^\circ$  were selected. Several interesting characteristics may be noticed. First, the two functions are slightly different, since they do not only depend on the absorption by ozone, but also on the scattering in the atmosphere (probability  $p$  in Eq. 2), which in turn depends on polarisation. Differences between  $G_{par}$  and  $G_{per}$  can be as large as 50% for SZAs in the range  $75^\circ - 95^\circ$ , which highlights the importance of polarisation effects in the simulations. For example,  $G_{par}$  is slightly larger than  $G_{per}$  due to the longer path in the atmosphere for multiple-scattered photons. Indeed, when the RTM is run in single-scattering mode (Fig. 4), the resulting  $G'_{par}$  and  $G'_{per}$  coincide (although the absolute  $I'(\lambda)$  are different due to the polarising properties of the Rayleigh scattering) and are lower than in the previous case. Indeed, in the single scat-

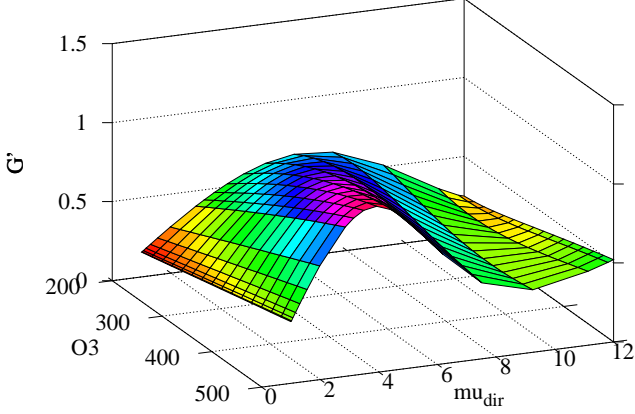


Figure 4: Matrix  $G$  in the single scattering approximation.

tering approximation, a photon can reach the detector only after travelling straight in the atmosphere, then vertically to the detector, and the probabilities related to this path in both polarisations are equal. The vertical crossing of the atmosphere also contribute to the shorter optical path. Second, the function is strictly increasing with ozone at low SZAs, then it starts saturating at larger SZAs, especially for high ozone VCDs. The saturation effect was already noticed by Fioletov et al. (2011). However, we are now extending the analysis to AMFs greater than 6 (in contrast to previous publications) and another feature is revealed: the function reverses and starts decreasing with ozone at higher SZAs. Finally, for extremely large AMFs,  $G$  is again increasing with ozone. Further simulations reveal that the exact position of the reversal depends both on the ozone profile and, to a lesser extent, on the weightings of the linear combination, but this feature cannot be removed from  $G$ . This behaviour can be problematic for the ozone retrieval in the ZS geometry, since  $G$  is not accurately invertible for a range of SZAs, i.e. the incoming radiation carries little information about ozone. It is important to note that the spectral irradiance at a single wavelength always decreases for increasing ozone VCD, therefore the feature is to ascribe to the linear combination, i.e. to the ratio of spectral irradiances.

This behaviour is to ascribe to the well-known Umkehr effect (Götz et al., 1934). When the sun is near the horizon, if a ratio of the zenith irradiances recorded at two different wavelengths, one strongly absorbed by ozone and the other weakly absorbed, is plotted against the SZA, it is observed that this log-intensity ratio decreases as the zenith angle increases until a minimum (maximum, in our study, owing to the way  $G$  was defined) is reached for a specific zenith angle. The exact SZA depends on the ozone profile, since photons at different wavelengths are scattered from different altitudes to the receiver (the lower wavelength is scattered from a higher altitude, since strong absorption inside the ozone layer occurs at lower altitude; conversely, larger wave-

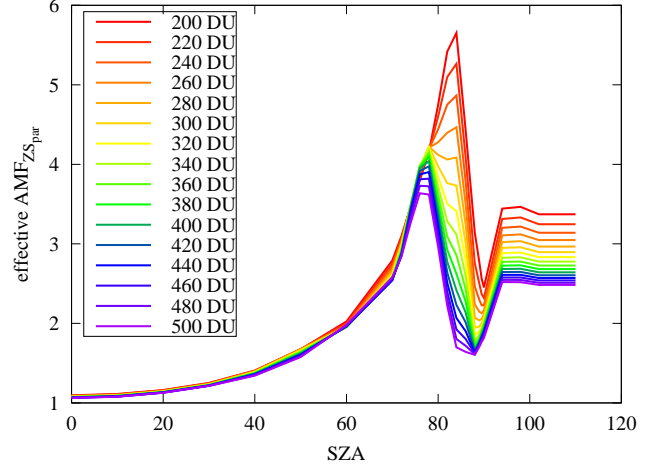


Figure 5: Effective AMF for ZS observations, parallel polarisation, as a function of the SZA and ozone VCD.

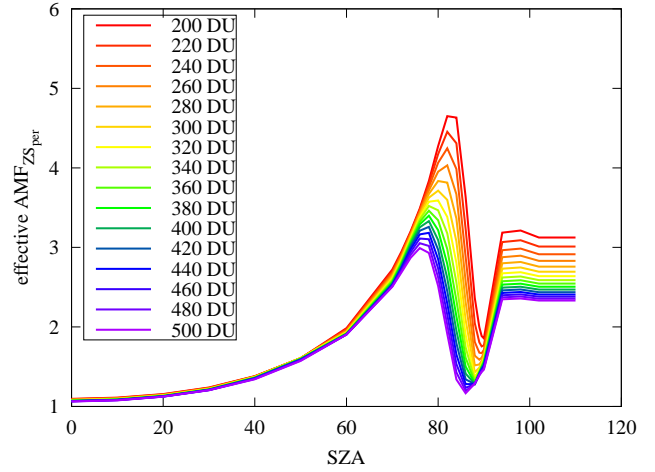


Figure 6: Effective AMF for ZS observations, perpendicular polarisation, as a function of the SZA and ozone VCD.

lengths are scattered at lower altitudes, since pressure - and, therefore, Rayleigh scattering - is larger near the ground). Since the ozone profile generally shows a maximum at a defined height in the stratosphere, the ratio of the irradiance logarithms at two wavelengths (or, equivalently, the linear combination of the log-intensities at several wavelengths) reverses.

We now try to calculate an effective AMF for ZS observations, i.e. we test whether Eq. 2 can be reduced to Eq. 3. To this purpose, we divide  $G$  by the linear combination of the ozone optical depth along the vertical. Figures 5 and 6 may be seen as versions of Figs. 2 and 3 rescaled and viewed from one side. Again, it can be noticed that the effective AMF is generally higher for the parallel polarisation compared to the perpendicular polarisation owing to the longer path followed by multiple-scattered photons. What we want to underline

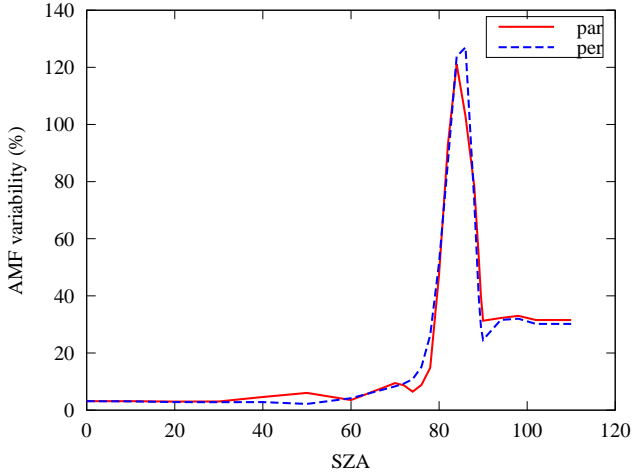


Figure 7: Variability (maximum - minimum range) of the effective zenith AMFs due to dependence on ozone.

here is that, due to the non-linearity of  $G$  with respect to the ozone VCD, the effective AMF is generally a function of ozone as already reported, for example, by Marquard et al. (2000), thus it cannot be employed to determine the ozone in a trivial way. At least, an iterative procedure, similarly to the formulation by Rozanov and Rozanov (2010), should be adopted in the range where  $G$  is invertible (though not linear with the ozone VCD). The higher AMF for lower ozone VCDs may be explained owing to the fact that photons can travel a longer path in the atmosphere before being absorbed if the ozone concentration is lower. Figure 7 shows the percentage variability of the effective AMFs due to the ozone dependence (over the full range 200–500 DU). The range of variability is about 3% for SZAs lower than about 40°, then remarkably increases, especially for SZAs larger than 70°, where the deviations from the linearity of  $G$  cannot be neglected. Obviously, if an *a priori* ozone climatology is known (e.g., from DS observations), the full range of 200–500 DU can be reduced and the variability decreases.

The ratio between the effective ZS AMFs in both polarisations and the geometrical calculation in the DS case is depicted in Figs. 8 and 9. Two considerations are worth particular attention. First, the ratio is always larger than unity at low SZAs, even when the sun is close to the zenith. The role of multiple scattering of diffuse light in this phenomenon is easy to prove: if multiple scattering is switched off in the model, then the ratio nicely goes to unity for SZAs close to 0; moreover, it can be noticed that the deviations from unity are higher for lower ozone VCDs, since photons are less absorbed and free to travel in the atmosphere along the zenith direction. Multiple scattering is not considered in the DS geometry and DS AMF calculations are only based on geometrical considerations without using RTMs. However, the effect of multiple scattering on the AMF is expected to be negligible since diffuse light

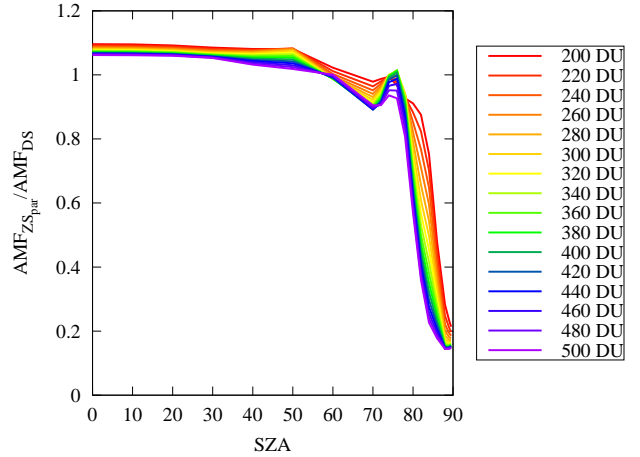


Figure 8: Ratio between ZS (parallel polarisation) and DS AMFs.

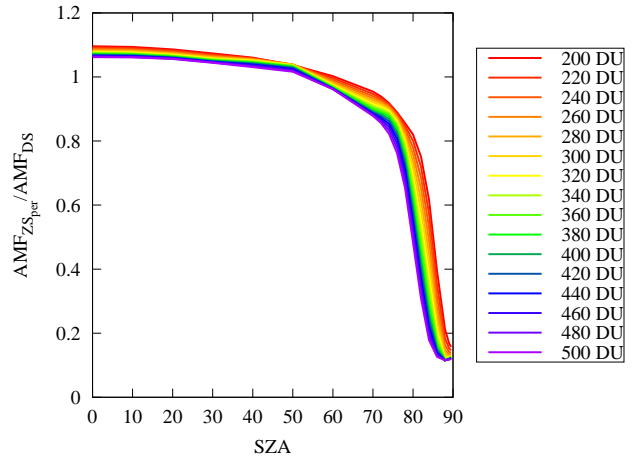


Figure 9: Ratio between ZS (perpendicular polarisation) and DS AMFs.

represents a small fraction of the measured irradiance in this observation geometry. The second feature in the figures is that the ZS AMFs are lower than the DS AMFs for SZAs larger than about 60°. This effect is quite counterintuitive, since we expect that diffuse light at the zenith travels more than the direct light. We should recall that the effective AMF was calculated from the linear combination and is thus only representative of the absorption in the ozone layer (other effects were removed by the linear combination). At large SZAs, the only way diffuse photons have to reach the detector without being absorbed by ozone is to travel above the ozone layer and be scattered vertically down to the Brewer, which results in a shorter effective AMF, while the direct beam penetrates obliquely the ozone layer.

The Brewer sensitivity,  $\frac{dG}{dX}$  (Eq. 6), is reported in Figs. 10 and 11. The derivative was calculated by the finite differences method by perturbing the model (3

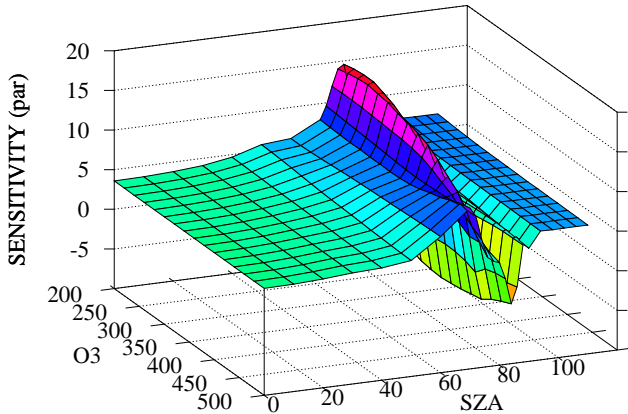


Figure 10: R6 sensitivity to a change in the ozone VCD of 1 DU (parallel polarisation).

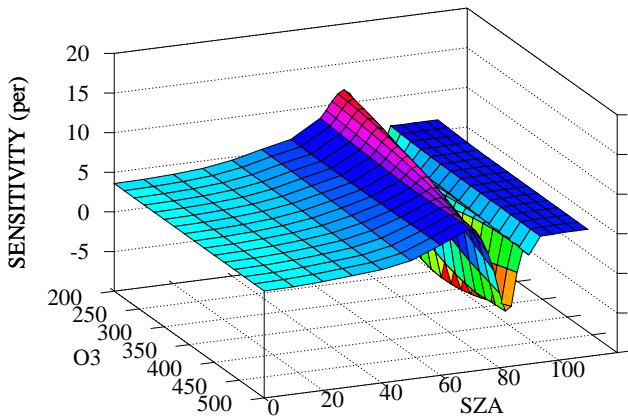


Figure 11: R6 sensitivity to a change in the ozone VCD of 1 DU (perpendicular polarisation).

DU were added to the ozone VCD). The values shown in the figures are additionally multiplied by a factor  $10^4/\ln(10)$  for comparison with the R6 sensitivity in the DS geometry. A sharp change in the sign of the sensitivity can be noticed in the Umkehr zone. ZS Brewer retrievals cannot be performed in regions where the sensitivity cross the zero of the Z-scale due to a loss of sensitivity.

## 5.2 Example of a ZP Langley

October 7 was chosen as one of the best days of the campaign for a Langley extrapolation, with an unperturbed sky and very stable ozone of about 258 DU from DS measurements. We will analyse the ZP data from Brewer #145 for this day as a proof-of-concept of the effectiveness of the new algorithm. Obviously, an accurate Langley calibration should make use of a larger number of observations for statistics purposes which would require a much longer measurement period.

The main limitation of a Langley plot with the new formulation is that the airmass, which is necessary for

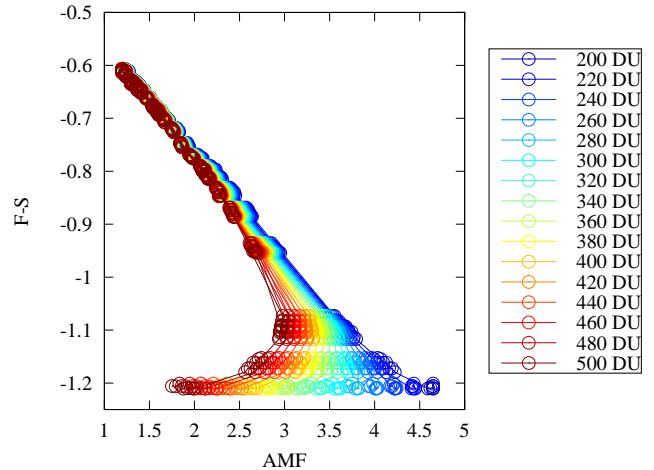


Figure 12: Langley plot for day 280 and ZP measurements.

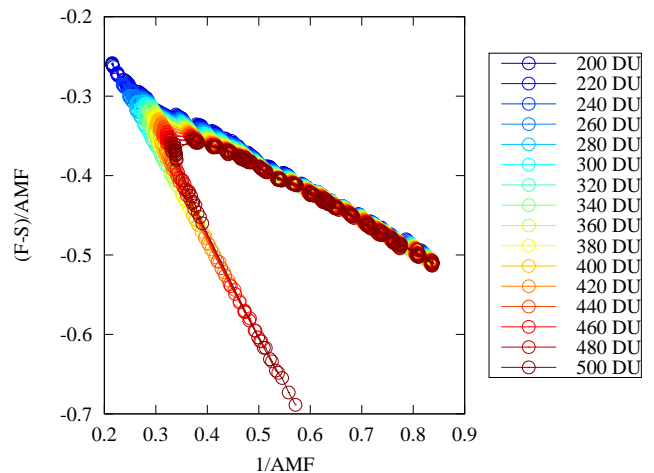


Figure 13: Langley plot for day 280 and ZP measurements (alternative formulation using the inverse AMF).

the Langley plot, is a function of the (unknown) ozone VCD. Two solutions will be proposed further in the text. A first method consists in performing several Langley plots, each one with a different *a priori* ozone VCD for the calculation of the AMF. Then, the “best” plot is chosen according to some criteria. The working hypothesis is that the ozone content is constant throughout the day. Equation 5 was slightly modified to take into account a calibration factor, *ETC*, summarising the spectral sensitivity of the specific Brewer and the terms were rearranged:

$$F(\theta, X) - S(\theta) = ETC - G(\theta, X) \quad (10)$$

Then,  $F(\theta, X) - S(\theta)$  was plotted as a function of the airmass (Fig. 12). An equivalent plot is provided in Fig. 13 as a function of the inverse AMF, as also used in the scientific literature (e.g. Adler-Golden and Slusser, 2007). Non-linearities occur in both figures when the

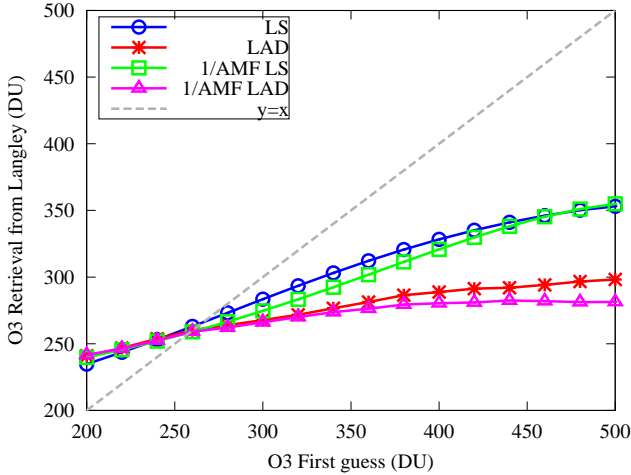


Figure 14: Ozone retrieved from the slope of the Langley fit as a function of the initial guess used for AMF calculations.

first guess of ozone is too different from the actual value. This can be used as a criterium to select the proper ozone value. For example, the Pearson's correlation coefficient is best for an initial estimate of 240 DU ( $\rho = -1.000$ ) and worse for a first estimate of 500 DU ( $\rho = -0.839$ ), with a value of  $\rho = -0.999$  when the first guess corresponds to the ozone VCD from DS retrievals. Alternatively, the differences between the first guess and the ozone retrieved from the slope of the Langley regression line could be analysed to determine the best estimate. To this purpose, several methods were used to perform the fit: least squares (LS), least absolute deviations (LAD), LS with 1/AMF formulation and LAD with 1/AMF formulation. The best agreement between the *a priori* ozone and the retrieval is reached for an initial guess of 260 DU, which corresponds to a Langley slope of 263 DU (LS), 260 DU (LAD), 259 DU (1/AMF LS) and 259 DU (1/AMF LAD). The dependence between the first guess and the retrieval is presented in Fig. 14, which interestingly shows that an iterative procedure could also be employed since the determination of the ozone VCD converges: if the initial guess is lower than the actual one, then the retrieval will increase the *a priori* value and viceversa.

The retrieved *ETC* (intercept of the regression line) for ZP measurements during this day is about -0.35 (in natural logarithm units) and slightly depends on the fitting method. The *ZP ETC* approximately corresponds to the DS calibration constant, -0.3638 (1580 in the log10 units usually used in the operating software). It should be noticed, however, that the extraterrestrial constants for DS and ZS geometries could slightly differ, since different combinations of filters (neutral density and diffuser/polariser) are used.

We have now the *ETC* and an overall estimate of the mean ozone VCD for the full day and we can easily perform the retrieval for each Brewer measurement by

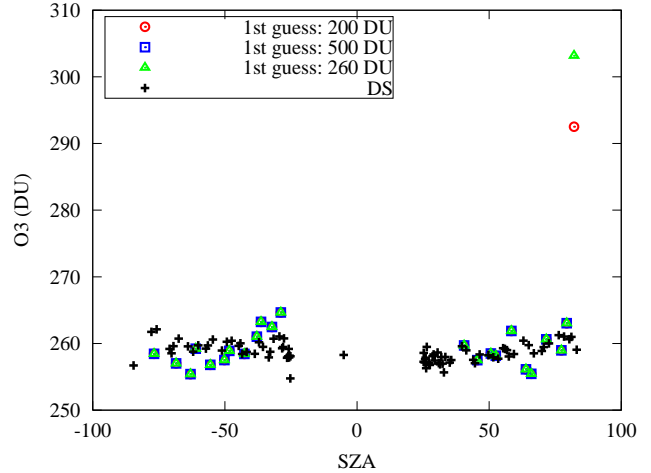


Figure 15: ZS and DS retrievals as a function of the SZA (negative SZAs: morning; positive: afternoon). The first-guess values are reported in the legend. An iterative method was used for the 200 and 500 DU cases.

inverting Eq. 10. Figure 15 shows the results of the ZS retrieval for an *a priori* ozone VCD of 260 DU (green triangles markers) together with the estimate from DS measurements (black crosses) as a function of the SZA. The mean and the median of the differences between the two geometries are -0.15 and -0.11 DU, respectively. The root mean square difference (RMSD) is 2.7 DU. This can be considered a promising result, according to the fact that only one day was employed to determine the *ETC*. The good comparison, however, is also due to the favourable location of MLO, where the actual ozone profile is very close to the one provided to the radiative transfer model.

In this case, the retrieval was performed using the AMF calculated on the basis of a truthful ozone VCD, obtained from the slope of the Langley regression. However, in normal measurements, the ozone can vary during the day or only few samples can be available throughout the full day, so that a Langley plot cannot be performed. Figure 16 depicts the importance of the *a priori* value for the AMF calculations. Differences in the resulting retrievals can be larger than 20 DU, especially in the range of larger variability of the AMF (Fig. 6). An iterative procedure was therefore chosen:

1. we start from a first guess corresponding to a climatological value;
2. the relative AMF was calculated as a function of the SZA and first ozone estimate;
3. we retrieve the ozone by inverting Eq. 10;
4. we update the *a priori* ozone and start the procedure again;
5. the iteration is repeated 10 times. As an alternative, a convergence criterium can be assessed.

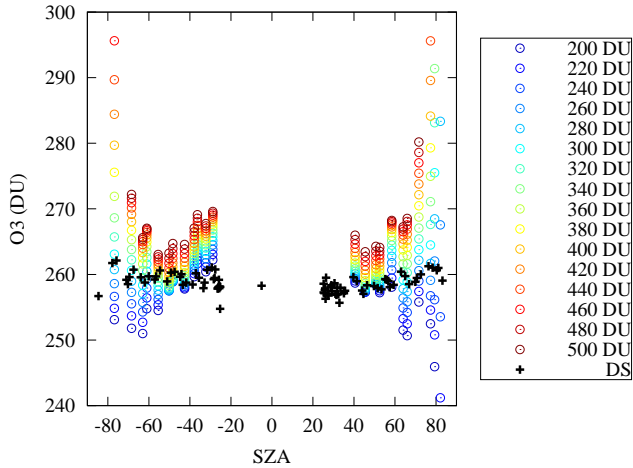


Figure 16: ZS retrievals as a function of the SZA and the first guess needed to calculate the AMF. The DS estimates are also reported for comparison purposes.

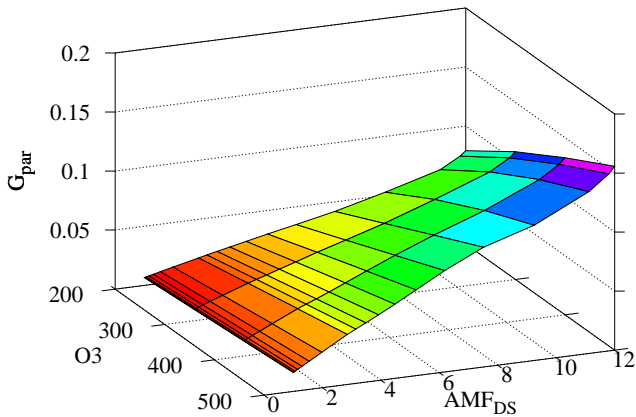


Figure 17: Matrix  $G$  in parallel polarisation for the Umkehr grating position.

Figure 15 shows that the method converges and provides very accurate estimates, even in the extreme cases where the *a priori* was selected at the limit of the range (200 and 500 DU). Only one point, at a SZA of about  $82^\circ$ , diverges if the initial guess is too large (500 DU), probably owing to the anomalous Brewer sensitivity changes at the SZA where the Umkehr effect manifests. Moreover, convergence in the case of MLO does not imply that the method works at other, and more challenging, stations.

### 5.3 Measurements at higher wavelengths

To avoid loss of sensitivity by the Brewer and large uncertainties triggered by the Umkehr effect and the unknown ozone profile, we studied the performances of the algorithm when the measuring spectral range is shifted towards larger wavelengths. Indeed, the issues

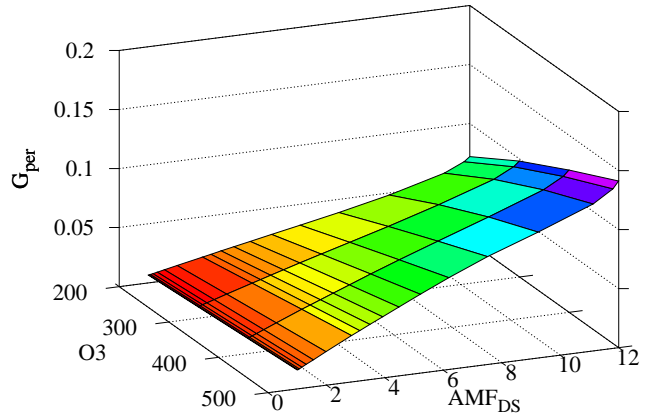


Figure 18: Matrix  $G$  in perpendicular polarisation for the Umkehr grating position.

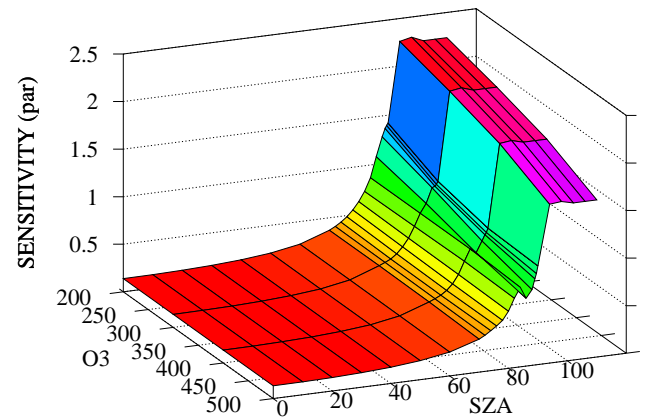


Figure 19: R6 sensitivity to a change in the ozone VCD of 1 DU (parallel polarisation and Umkehr grating position).

are mainly due to a too strong absorption by ozone. Conversely, at larger wavelengths, the ozone absorption decreases and the problem is expected to converge to an easier retrieval of a weak absorber. This is probably the reason why other instruments performing zenith sky observations, such as the *Système d'Analyse par Observation Zénithale* (SAOZ) (e.g., Hendrick et al., 2011)), employ the Chappuis band in the visible spectral range and the definition of an effective AMF together with the BLB equation.

Hence, the matrices  $S$  and  $G$  were recalculated for different sets of wavelengths corresponding to different positions (microsteps) of the Brewer grating. Only the range accessible by single monochromator instruments was explored to ensure that the algorithm is compatible with all Brewer models. The spectral range was divided in regular intervals at fixed steps and the weightings were recalculated at each step to ensure correct removal of interfering factors, as in the standard algorithm. Generally, as the wavelength increases, the region of the

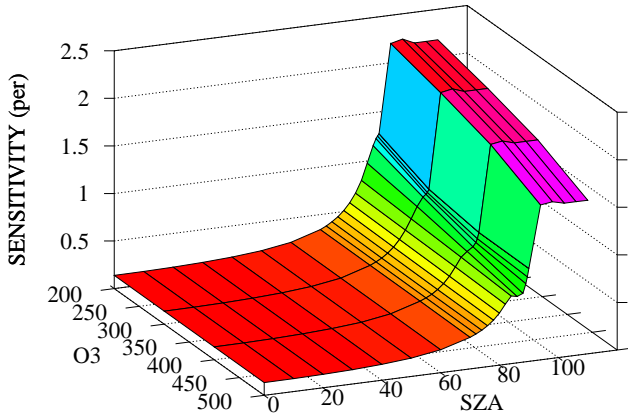


Figure 20: R6 sensitivity to a change in the ozone VCD of 1 DU (perpendicular polarisation and Umkehr grating position).

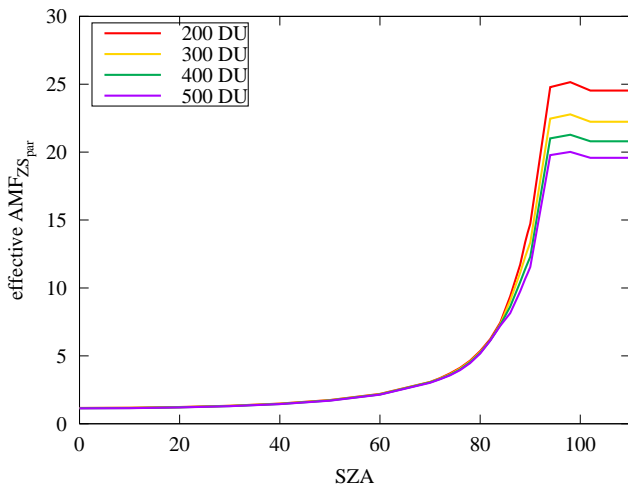


Figure 21: Effective AMF for ZS observations, parallel polarisation and Umkehr grating position.

Umkehr effect is shifted towards higher SZAs. However, the results are perturbed by the rapidly changing ozone cross section with wavelength and, since the chosen sets of wavelengths are not optimised (but simply the result of a regular grid in the grating microsteps space), the shape of  $G$  abruptly changes from one microstep to the other. The sensitivity is also reduced at wavelengths where the differential structure of the ozone cross section is very weak.

We therefore focused on only one grating position in the register of larger wavelengths, i.e. the one used by the Umkehr routine. The resulting set of wavelengths is well defined on every Brewer, since it is chosen in order that the wavelength corresponding to the first slit with the grating in the new position corresponds to the wavelength of the sixth slit at the default position. Moreover, this position guarantees that the differential structure of the ozone cross sections is well captured. A

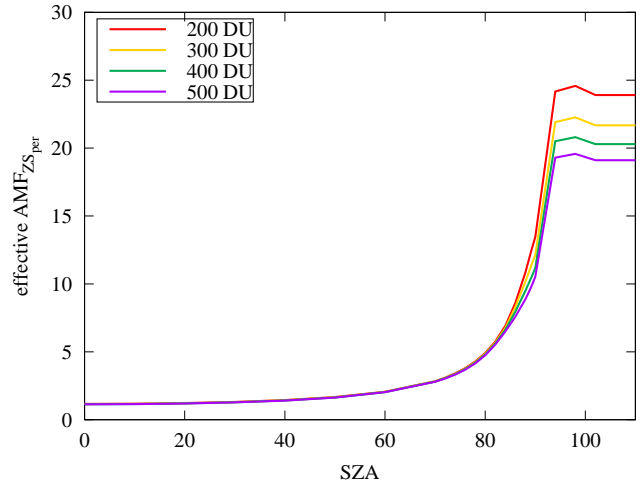


Figure 22: Effective AMF for ZS observations, perpendicular polarisation and Umkehr grating position.

new routine was developed (`zu.rtn`) and can be used by the Brewer community. The routine not only moves the grating to microsteps corresponding to larger wavelengths, but it also turns the tracker perpendicularly to the sun.

With this grating position, however, the ozone cross sections corresponding to the last four slits are almost linear with wavelength and the Brewer sensitivity dramatically drops, since the vector of the weightings becomes almost perpendicular to the ozone cross section vector. To overcome this issue, we decided to use the spectral irradiances measured through all six slits (measurements through the first two slits are now more accurate, since the solar flux is higher at larger wavelengths) and take advantage of the additional degrees of freedom to maximize the signal by ozone. This is automatically accomplished when calculating the weighting factors by the single value decomposition (SVD) algorithm when the system is underconstrained. Figures 17 and 18 show the corresponding  $G$  matrices for both polarisations. The benefit of the new grating position is that the Umkehr effect has disappeared. However, as a side effect, the sensitivity has remarkably decreased at low SZAs (Figs. `reffig:sensparU` and 20), while it is still sufficiently high at large SZAs. The new technique is therefore complementary to the standard method and could efficiently be used when the sun is low on the horizon (e.g., during twilight) to avoid the Umkehr effect. Conversely, due to the weak absorption by ozone at larger wavelengths, the ozone signal at low SZAs is better detected by the old method.

The effective AMFs for the new set of wavelengths are much larger than before (Figs. 21 and 22), since photons can travel a longer path in the atmosphere before being absorbed. The magnitude of the new AMFs recalls the results obtained for nitrogen dioxide retrievals in the visible range (e.g., Diémoz et al., 2014). Above all, the

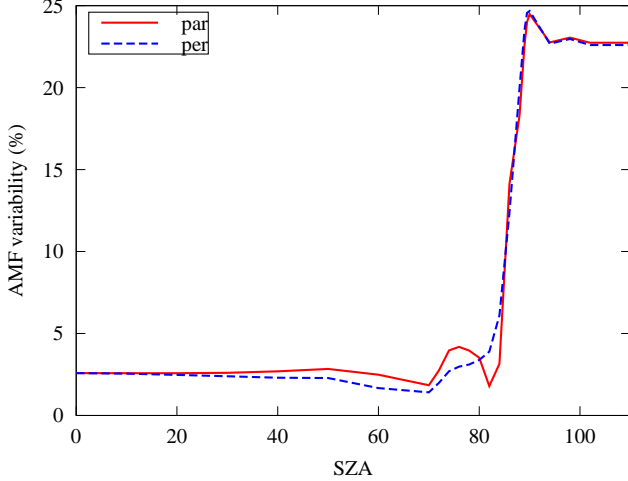


Figure 23: Variability (maximum - minimum range) of the effective zenith AMFs due to dependence on ozone (Umkehr grating position).

AMF variability due to the dependence on ozone is reduced (Fig. 23), which allows to define an effective AMF and use a BLB-like equation for the retrieval.

The experimental results of the ZU Langley at MLO and the corresponding ozone retrievals are currently under investigation.

#### 5.4 Additional studies

Two additional studies were performed during the STSM. In the first one, we tried to understand whether and how it is possible to determine, using only one Brewer spectrophotometer, if the atmosphere is sufficiently stable for a Langley calibration. The issue arises from the fact that variations in the ozone VCD centred at the local noon can apparently result in perfectly straight Langley plots, however the *ETC* can be erroneous (Marengo, 2007). One example is the following, where the ozone optical depth varies as a function of the inverse of the AMF ( $\mu$ ):

$$\tau = \tau_0 + \frac{\Delta}{\mu} \quad (11)$$

$\tau_0$  represents an “average” value and  $\Delta$  the magnitude of the daily variation. The resulting BLB equation will be

$$\begin{aligned} \log I &= \log I_0 - \mu \left( \tau_0 + \frac{\Delta}{\mu} \right) \\ &= (\log I_0 - \Delta) - \mu \tau_0 \end{aligned} \quad (12)$$

i.e., a straight line with an intercept equal to  $\log I_0 - \Delta$ . We tried to calculate how this effect appears in different geometries, e.g. DS and ZS. The advantage of observations in two geometries is that the AMF dependence on the SZA is different, therefore ozone

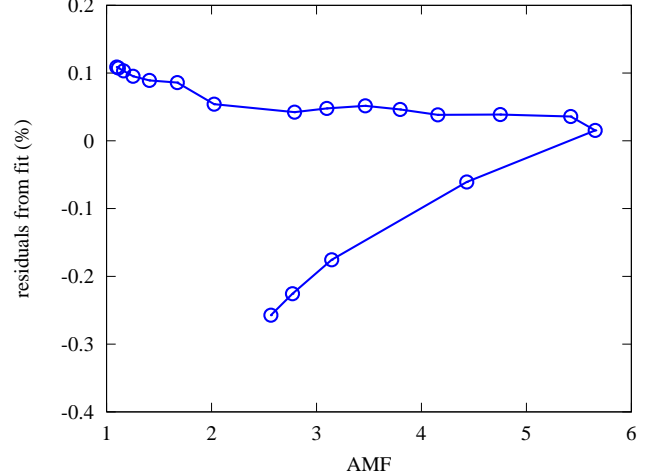


Figure 24: Residuals from the Langley ZS regression line owing to an ozone variation of 1% throughout the day.

variations that can easily “fool” one geometry may be discovered in the other. For example, if the ozone optical depth varies as a function of the DS AMF (Eq. 11), Eq. 12 for ZS estimates will be

$$\begin{aligned} \log I &= \log I_0 - \mu_{ZS} \left( \tau_0 + \frac{\Delta}{\mu_{DS}} \right) \\ &= \log I_0 - \Delta \frac{\mu_{ZS}}{\mu_{DS}} - \mu_{ZS} \tau_0 \end{aligned} \quad (13)$$

which, in principle, does not result in a straight line. The ratio between the AMFs in two different geometries appearing in the above equation was already plotted in Figs. 8 and 9. Figure 24 presents the residuals from the Langley ZS regression line owing to an ozone variation of 1% throughout the day.

A second study deals with ZS retrievals at very high latitudes in the Southern Hemisphere. Indeed, some users noticed negative ozone concentrations from the ZS retrievals using the standard algorithm during the ozone hole period. To understand this phenomenon, the inversion matrices were recalculated using an ozone profile measured at the South Pole with a balloon by NOAA on October 3, 2015 (i.e., during the ozone hole conditions, Fig. 25) and a surface albedo of 0.90. As expected, the differences between the new matrices and those found for MLO conditions are obvious (Figs. 26 and 27) and even larger than 50% for some SZAs. The negative retrievals could arise from the use of a standard set of polynomials for a very peculiar ozone profile.

## 6 Conclusions

The results presented in this report are very preliminary. Further research is needed on the following topics:

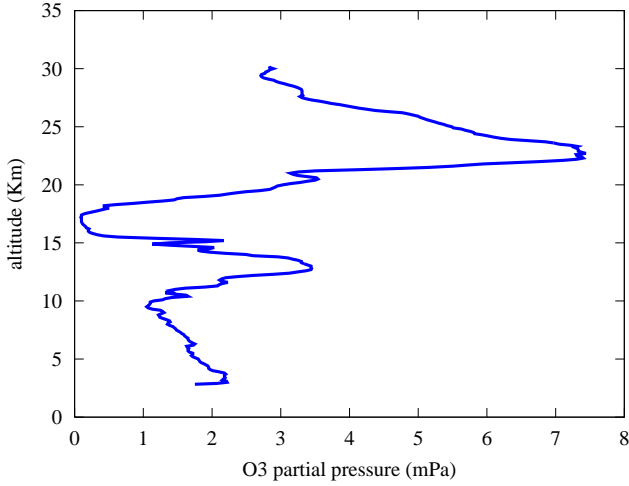


Figure 25: Ozone profile during ozone hole conditions, from a balloon sonde at the South Pole (NOAA).

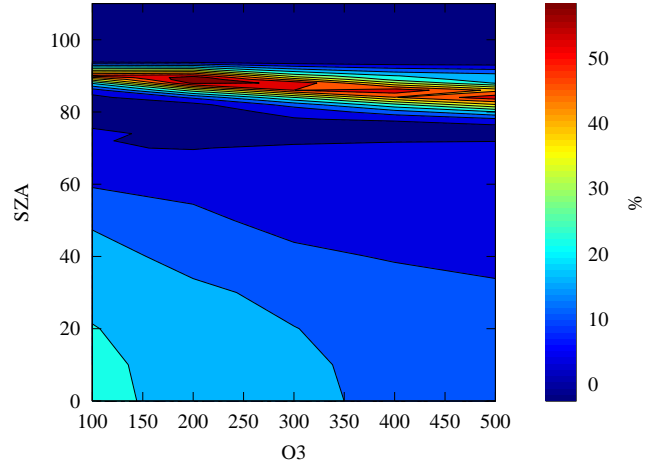


Figure 27: Differences between  $G$  matrices in perpendicular polarisation calculated for MLO and the South Pole during ozone hole conditions.

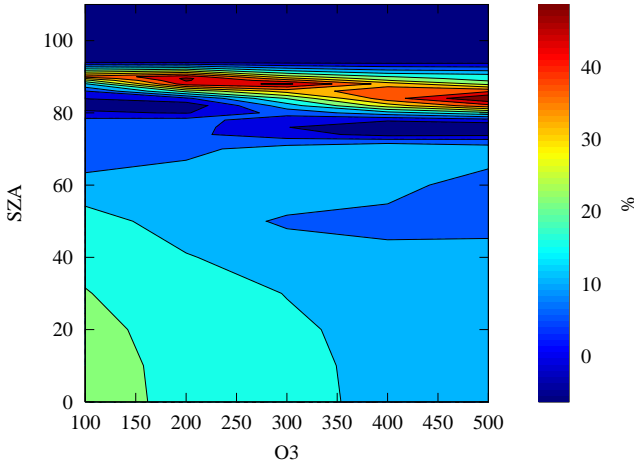


Figure 26: Differences between  $G$  matrices in parallel polarisation calculated for MLO and the South Pole during ozone hole conditions.

1. physics of zenith sky observations: a better understanding of the way the Umkehr effect influences the retrieval is needed. Use of a single-scattering model to calculate the effective scattering height for each wavelength will provide an intuitive, but useful, explanation. Moreover, further research must be performed to compare ozone retrievals between different geometries owing to different paths and regions sounded in the atmosphere;
2. sensitivity analysis: how do clouds and aerosol perturb the ZS/ZP/ZU retrieval? How is the retrieval affected by tropospheric ozone in polluted sites? Is the effect of rotational Raman scattering (Ring effect) evident for ZS observations? How can we remove this factor? Is there a “best” polarisation direction? Historically, the parallel polarisation was

chosen because the influence of clouds is weaker in principle, but does this correspond to measurements? Also, since more photons are measured in the perpendicular polarisation during twilight and the polarising filter inside the Brewer is not 100% effective, the perpendicular polarisation could be convenient;

3. data analysis: Langley plots and retrievals with ZU data; processing of multiple days and comparison with DS observations on a longer period; analysis of measurements performed during cloudy days; processing of the ZS and ZP data series in Izaña and low-altitudes stations (e.g., Aosta, Toronto); comparison between different Brewer models (MkIII, MkII and MkIV) using data collected during the campaign at MLO with ZS, ZP and ZU to assess the influence of straylight. Considerations about the spectral AMFs instead of the linear combination of AMFs (as done in the present work) could help in identifying the actual optical path length in the atmosphere;
4. algorithm implementation: calculation of an optimised grating position at larger wavelengths to improve the sensitivity to ozone. Check whether slight changes in the measuring wavelength can be compensated by simply recalculating the differential absorption coefficient, as done during ozone calibration services, rather than fully updating the inversion matrices,  $G$ .

The collaboration with the hosting institution, International Ozone Services, is expected to continue and strengthen in the future. At least one scientific article about the new ZS methodology will be submitted to an international journal as soon as the present study is completed. Other interesting research topics are connected to this study, such as the Umkehr technique and

other troposphere-stratosphere partitioning methods. Therefore, the results obtained on ZS retrievals could serve as the basis to improve other techniques as well.

## 7 Acknowledgements

I would like to gratefully acknowledge the EUBREWNET COST Action for the financial support and the National Oceanic and Atmospheric Administration (NOAA) for hosting me at the Mauna Loa Observatory facilities. Furthermore, I must sincerely thank my Canadian hosts, Volodya and Mike. I learned a lot from their scientific and technical expertise. They treated me as a brother and welcomed me in Hawaii with unique human warmth.

## References

- Adler-Golden, S. and Slusser, J.: Comparison of plotting methods for solar radiometer calibration, *J. Atmos. Ocean. Tech.*, 24, 935–938, doi:10.1175/JTECH2012.1, 2007.
- Bass, A. and Paur, R.: The Ultraviolet Cross-Sections of Ozone: I. The Measurements, in: *Atmospheric Ozone*, edited by Zerefos, C. and Ghazi, A., pp. 606–610, Springer Netherlands, doi:10.1007/978-94-009-5313-0\_120, 1985.
- Bouguer, P.: *Essai d’optique sur la gradation de la lumière*, 1729.
- Brühl, C. and Crutzen, P. J.: MPIC two-dimensional model, *NASA Ref. Publ.*, 1292, 103–104, 1993.
- Diémoz, H., Siani, A. M., Redondas, A., Savastiouk, V., McElroy, C. T., Navarro-Comas, M., and Hase, F.: Improved retrieval of nitrogen dioxide (NO<sub>2</sub>) column densities by means of MKIV Brewer spectrophotometers, *Atmos. Meas. Tech.*, 7, 4009–4022, doi:10.5194/amt-7-4009-2014, 2014.
- Dobson, G.: *Observers’s handbook for the ozone spectrophotometer*, *Ann. Int. Geophys. Year*, 5, 46–89, 1957.
- Fioletov, V. E., McLinden, C. A., McElroy, C. T., and Savastiouk, V.: New method for deriving total ozone from Brewer zenith sky observations, *J. Geophys. Res.*, 116, doi:10.1029/2010JD015399, d08301, 2011.
- Götz, F. W. P., Meetham, A. R., and Dobson, G. M. B.: The Vertical Distribution of Ozone in the Atmosphere, *Proc. Royal Society of London*, 145, 416–446, URL <http://www.jstor.org/stable/2935512>, 1934.
- Gröbner, J., Wardle, D. I., McElroy, C. T., and Kerr, J. B.: Investigation of the wavelength accuracy of Brewer spectrophotometers, *Appl. Optics*, 37, 8352–8360, 1998.
- Hendrick, F., Pommereau, J.-P., Goutail, F., Evans, R. D., Ionov, D., Pazmino, A., Kyrö, E., Held, G., Eriksen, P., Dorokhov, V., Gil, M., and Van Roozendaal, M.: NDACC/SAOZ UV-visible total ozone measurements: improved retrieval and comparison with correlative ground-based and satellite observations, *Atmos. Chem. Phys.*, 11, 5975–5995, doi:10.5194/acp-11-5975-2011, 2011.
- Kerr, J., McElroy, C., and Olafson, R.: Measurements of ozone with the Brewer spectrophotometer, in: *Proc. Quadrennial International Ozone Symposium*, 1981.
- Langley, S. P.: The bolometer and radiant energy, in: *Proc. American Academy of Arts and Sciences*, vol. 16, pp. 342–358, JSTOR, 1880.
- Marenco, F.: On Langley plots in the presence of a systematic diurnal aerosol cycle centered at noon: A comment on recently proposed methodologies, *J. Geophys. Res.*, 112, doi:10.1029/2006JD007248, URL <http://dx.doi.org/10.1029/2006JD007248>, d06205, 2007.
- Marquard, L. C., Wagner, T., and Platt, U.: Improved air mass factor concepts for scattered radiation differential optical absorption spectroscopy of atmospheric species, *J. Geophys. Res.*, 105, 1315–1327, doi:10.1029/1999JD900340, 2000.
- Muthama, N. J., Scimia, U., Siani, A. M., and Palmieri, S.: Toward optimizing Brewer zenith sky total ozone measurements at the Italian stations of Rome and Ispra, *J. Geophys. Res.*, 100, 3017–3022, doi:10.1029/94JD02389, 1995.
- Rozanov, V., Rozanov, A., Kokhanovsky, A., and Burrows, J.: Radiative transfer through terrestrial atmosphere and ocean: Software package SCIATRAN, *J. Quant. Spectrosc. Ra.*, 133, 13 – 71, 2014.
- Rozanov, V. V. and Rozanov, A. V.: Differential optical absorption spectroscopy (DOAS) and air mass factor concept for a multiply scattering vertically inhomogeneous medium: theoretical consideration, *Atmos. Meas. Tech.*, 3, 751–780, doi:10.5194/amt-3-751-2010, 2010.
- Slusser, J., Gibson, J., Bigelow, D., Kolinski, D., Disterhoft, P., Lantz, K., and Beaubien, A.: Langley method of calibrating UV filter radiometers, *J. Geophys. Res.*, 105, 4841–4849, doi:10.1029/1999JD900451, 2000.
- Solomon, S., Schmeltekopf, A. L., and Sanders, R. W.: On the interpretation of zenith sky absorption measurements, *J. Geophys. Res.*, 92, 8311–8319, doi:10.1029/JD092iD07p08311, 1987.